Quick Spectrometric Characterization of Monolithic Perovskite Silicon Tandem Solar Cells Using Monochromatic Light Sources

Oliver Fischer,* Alexander J. Bett, Khusan Abrorov, Mohamed A. A. Mahmoud, Florian Schindler, Stefan W. Glunz, and Martin C. Schubert*

In monolithic perovskite silicon dual-junction solar cells, it is crucial that the subcells are current-matched to maximize performance. The most precise method to determine the current (mis)match of a monolithic dual-junction solar cell is a spectrometric measurement with, e.g., a light-emitting diode (LED)-based solar simulator. However, recoding multiple current voltage curves (*IV* curves) under different red- and blueshifted spectra relative to the AM1.5g reference spectrum is time-consuming. Herein, a new method is suggested to quickly test solar cells for current mismatch. A solar simulator with two lasers instead of multiple LEDs is used, so that two monitor diodes can track intensity changes of each light source during the measurement. Postmeasurement corrections can be applied using this data, circumventing long stabilization times of the solar simulator. To minimize the scan time, it is focused only on determining the correct short-circuit current and not the full *IV* curve. The measurement method is validated comparing it to conventional spectrometric measurements using a stable III–V monolithic dual-junction solar cell. The measurement on the proof-of-concept setup shows a deviation of only 2.3% in the current at the current matching point compared to the reference measurement.

1. Introduction

Silicon solar cells have the highest market share of the global production.[1] However, the record efficiency of 27.3% for silicon solar cells is approaching the physical limit of 29.4% under the air mass 1.5 global (AM1.5g) spectrum.[2,3] Silicon-based tandem solar cells can help to overcome this intrinsic limit since they have lower thermalization losses compared to single-junction silicon solar cells. At the same time, thin film perovskite solar cells show high absorption coefficients[4] and have a flexible bandgap.[5–7] Perovskite silicon dual-junction solar cells with a record efficiency of 34.2% were recently reported.[2] Due to these properties, perovskite silicon dual-junction tandem solar cells are a promising candidate for future large-scale production.

Two-terminal monolithic perovskite silicon dual-junction solar cells have a simpler and cheaper solar cell stack design with fewer transparent electrodes and less complicated electrical connections in a module compared to three- or four-terminal dual-junction solar cells.[8,9] However, if the top and bottom solar cells are connected in series, the solar cell with the lower generated current determines the overall current of the tandem solar cell. It is therefore crucial to match the generated current in both subcells for the optimal performance. This current match also depends on the applied spectrum. A red- or blueshift relative to the AM1.5g spectrum will change the generated currents in the subcells.[10–13] Often, external quantum efficiencies (EQEs) multiplied by the AM1.5g spectrum are integrated to determine the generated current of the subcells.[13–20] However, the EQEs and the corresponding spectral responses S must be measured absolutely to allow their integration for the current determination. This is difficult for two-terminal dual-junction solar cells due to several effects that influence the EQE measurement, such as 1) the bias voltage to set the subcell under test under short-circuit current I_{SC} condition (in particular for solar cells with low parallel resistance R_p in the subcell under test, setting the correct bias voltage is crucial, but the essential bias voltage can only be estimated); 2) the bias illumination intensity; 3) a nonlinear behavior in the irradiance–current characteristics; and 4) transient effects in the perovskite subcell.[21–24] Spectrometric measurements do not depend on absolute EQEs and are hence more preferably used to determine the current matching point. This measurement technique has formerly been

O. Fischer, A. J. Bett, K. Abrorov, M. A. A. Mahmoud, F. Schindler,
S. W. Glunz, M. C. Schubert
Fraunhofer Institute for Solar Energy Systems ISE
Heidenhofstr. 2, Freiburg 79110, Germany
E-mail: oliver.fischer@ise.fraunhofer.de;
martin.schubert@ise.fraunhofer.de

O. Fischer, M. A. A. Mahmoud, S. W. Glunz
Chair for Photovoltaic Energy Conversion
Department of Sustainable Systems Engineering INATECH
University of Freiburg
Emmy-Noether-Str. 2, Freiburg 79110, Germany

applied to amorphous silicon dual-junction solar cells[25] and III–V multijunction solar cells.[10] In the meantime, it is applied to perovskite silicon dual-junction solar cells as well.[11,26–28] In spectrometric measurements, IV curves are measured under systematically blue- and redshifted spectra relative to the AM1.5g spectrum. Since a current mismatch decreases the short-circuit current of the tandem $I_{SC,tandem}$, the current matching point can then be determined by searching for the blue- or redshifted spectrum that maximizes $I_{SC,tandem}$. A detailed description on the measurement procedure for perovskite silicon dual-junction solar cells using a solar simulator based on light-emitting diodes (LEDs) is given by Bett et al.[11] and Er-raji, Messmer et al.[28] Since the stabilization of the solar simulator light source after a change of the spectrum as well as the measurement of the IV curve itself is time-consuming, a full spectrometric measurement is a lengthy process that can last several hours. This is a particular problem for tandem solar cells with a perovskite subcell since the speed of the IV sweep is limited by ion migration processes.[29] Given the problem of degradation of perovskites when exposed to humid air or oxygen during testing, a shorter measurement duration would be advantageous. Also, degradation or changes from the stabilized state of the solar cell during the measurements can impact the results and render them invalid for assessing the original solar cell. For inline characterization, where measurement throughput is crucial, this measurement technique needs to be accelerated as well.

In our work, we present a new measurement approach that solves this issue. Compromising on the number of different parameters that are acquired during the measurement in favor of measurement speed, only I_{SC} is determined for each spectrum. This drastically reduces the time that is usually needed for each full IV measurement sweep since only one instead of several hundreds of data points is acquired for each spectrum. In addition, two monochromatic light sources are used in our measurement approach instead of multiple LEDs with overlapping spectrum. These two light sources offer the advantage that two monitor diode units can constantly track the deviation of the actual laser power from the desired power. With this data on excitation light intensity, a correction can be applied to the measured current making the waiting time for light engine stabilization obsolete. This reduces the waiting time for the stabilization of the solar simulator, leading to a very fast measurement procedure to determine the current matching point within less than a minute.

2. Experimental Section

2.1. Measurement Setup

A measurement setup developed at Fraunhofer ISE and built by Intego GmbH is used for this work. A 450 nm laser subcell selectively excites the perovskite top cell. An 808 nm laser is used to excite the silicon bottom cell. The laser intensities are tracked live individually using two monitor diode units. A Keithley 2450 source measure unit (SMU) from Tektronix allows accurate current and voltage measurements. The measurement setup is displayed in **Figure 1**.
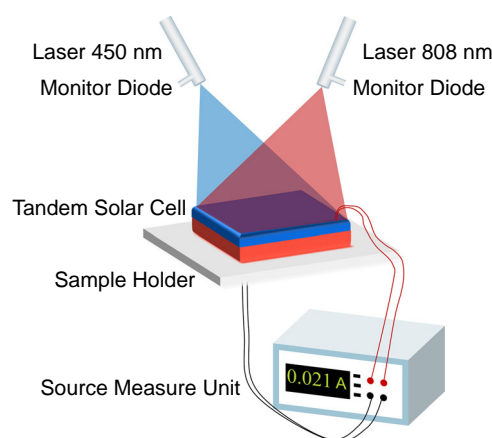

Figure 1. Schematic of the measurement setup. 450 and 808 nm lasers are used to excite the top and bottom solar cell of the dual-junction solar cell, respectively. The cell is contacted on a temperature-controlled sample holder. A SMU measures the short-circuit current I_{SC} of the solar cell. Two monitor diodes continuously track the laser output power.

2.2. Measurement Procedure

2.2.1. Determination of Spectrum

In a first step of the measurement procedure displayed in **Figure 2**, the relative spectral responses $s_{top}(\lambda)$ and $s_{bot}(\lambda)$ of the top and bottom subcells need to be measured. They differ from the absolute spectral responses $S_{top}(\lambda)$ and $S_{bot}(\lambda)$ that cannot be measured up to two unknown constants C_{top} and C_{bot} and it holds that $S_{top}(\lambda) = s_{top}(\lambda)\,C_{top}$ and $S_{bot}(\lambda) = s_{bot}(\lambda)\,C_{bot}$ for both
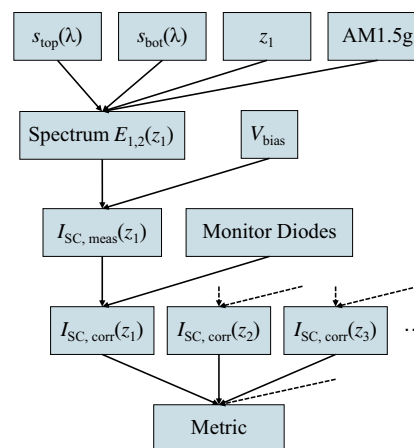

Figure 2. Schematic of the measurement procedure. The necessary simulator spectrum $e_{1,2}(z)$ is calculated with the help of the relative spectral responses of both subcells $s_{top}(\lambda)$ and $s_{bot}(\lambda)$. The spectral red- or blueshift is expressed with the parameter z relative to the AM1.5g spectrum. In a second step, $I_{SC}(z)$ of the limiting subcell is determined under the solar simulator spectrum, compensating for the effect of a low parallel resistance with a bias voltage V_{bias}. The as-measured short-circuit current $I_{SC,meas}(z)$ is corrected to the short-circuit current $I_{SC,corr}(z)$ compensating for unwanted intensity variations of the two light sources, which were detected with the two monitor diodes. This procedure is repeated for different spectral conditions z_1, z_2, ..., resulting in a quick spectrometric measurement.

subcells, respectively. In other words, while the shape of the as-measured spectral responses $s_{top}(\lambda)$ and $s_{bot}(\lambda)$ is correct, their magnitude needs to be rescaled using C_{top} and C_{bot} to obtain absolute spectral responses $S_{top}(\lambda)$ and $S_{bot}(\lambda)$. This holds true unless the spectral responses are affected by wavelength-dependent nonlinearities. Otherwise C_{top} and C_{bot} are no longer constants.

In the next step, the current densities under the AM1.5g spectrum $j_{top}^{AM1.5g}$ and $j_{bot}^{AM1.5g}$ of each subcell

$$j_{top/bot}^{AM1.5g} = \int S_{top/bot}(\lambda)E_{AM1.5g}(\lambda)d\lambda \tag{1}$$

are considered, where $E_{AM1.5g}(\lambda)$ is the AM1.5g spectrum in units of power per area per wavelength. We then introduce a parameter z following the approach of Meusel et al.[10] The parameter z describes a certain blue- or redshift of the (laser or LED based) solar simulator spectrum compared to the AM1.5g spectrum. The spectra are shifted in a way that the current densities j_{top}^{sim} and j_{bot}^{sim} that the subcells under test generate under the 1 sun equivalent simulator spectrum differ from $j_{top}^{AM1.5g}$ and $j_{bot}^{AM1.5g}$ according to

$$j_{top}^{sim} = (1+z)j_{top}^{AM1.5g} \tag{2}$$

$$j_{bot}^{sim} = (1-z)j_{bot}^{AM1.5g} \tag{3}$$

For the measurements we usually set $-0.2 \leq z \leq 0.2$. Note that (2) and (3) ensure that the sum of the ratio of the subcell currents $R_{top} = j_{top}^{sim}/j_{top}^{AM1.5g}$ and $R_{bot} = j_{bot}^{sim}/j_{bot}^{AM1.5g}$ stays always constant:[10]

$$R_{top} + R_{bot} = \frac{j_{top}^{sim}}{j_{top}^{AM1.5g}} + \frac{j_{bot}^{sim}}{j_{bot}^{AM1.5g}} = (1+z) + (1-z) = 2 \tag{4}$$

Depending on the tandem solar cell under test, it is possible that the light of one laser is not fully absorbed in one subcell but also contributes to the current in the other subcell. Hence, the linear equation system in Equation (5) and (6)[10] must be solved for the coefficients $A_{k,z}$ to determine the necessary laser spectra $E_{k,z}(\lambda)$ to generate the subcell currents j_{top}^{sim} and j_{bot}^{sim}.

$$\sum_{k=1}^{2} C_{top}A_{k,z}\int s_{top}(\lambda)e_k d\lambda = (1+z)C_{top}\int s_{top}(\lambda)E_{AM1.5g}(\lambda)d\lambda \tag{5}$$

$$\sum_{k=1}^{2} C_{bot}A_{k,z}\int s_{bot}(\lambda)e_k d\lambda = (1-z)C_{bot}\int s_{bot}(\lambda)E_{AM1.5g}(\lambda)d\lambda \tag{6}$$

Here, the spectrum of laser k is given by $E_{k,z}(\lambda) = A_{k,z}e_k(\lambda)$. e_k is the relative laser spectrum which we assume to have a Gaussian shape with a peak width of a few nanometers, as specified by the manufacturer. We use a silicon reference solar cell to calibrate the lasers, ensuring that their spectrum equals the desired spectrum $E_{k,z}(\lambda)$. Additionally, monitor diodes are calibrated with this silicon reference solar cell, enabling us to continuously track any deviations of the real laser spectrum from the desired spectrum $E_{k,z}(\lambda)$. Note that the knowledge of the absolute spectral response $S(\lambda)$ is not necessary to solve the equation system.

It is sufficient to know the relative spectral response $s(\lambda)$ up to the energy-independent scaling factors $C_{top/bot}$. This is important since the measurement of absolute spectral responses for dual-junction solar cells is affected by fundamental measurement artifacts as discussed above.

2.2.2. Current Measurement

Once the laser spectra are determined, the contacted sample can be illuminated with the two lasers. $I_{SC}(z)$ is then recorded for various spectra that correspond to different z. The different currents $I_{SC}(z)$ build up two groups: 1) the solar cell is limited by the top cell, and 2) the solar cell is limited by the bottom cell. $I_{SC}(z)$ can be fitted for both groups with a linear function. The intersection of the two linear functions marks the current matching point z_{match}. If $z_{match} < 0$, the tandem solar cell is limited under the AM1.5g spectrum by the silicon bottom cell and if $z_{match} > 0$, the tandem solar cell is limited by the perovskite top cell, respectively.

The operating voltage of the tandem solar cell in the field will be at the maximum power point (MPP). Hence, it is of interest whether the generated current of both subcells is matched for this condition. In contrast, the spectrometric measurement naturally is conducted under the I_{SC} condition with a terminal voltage of $V_{terminal} = 0$ V. This can be challenging for perovskite-based solar cells since I_{SC} may decrease over time under short-circuit condition due to degradation or ion movement.[28,30,31] This effect shifts the current matching point in a dual-junction solar cell as the short-circuit current of the silicon solar cell $I_{SC,bot}$ typically stays constant while the short-circuit current of the perovskite cell $I_{SC,top}$ may decay. Hence, we precondition the solar cell with a bias voltage close to MPP before the measurement starts to find the current matching point that applies to the field conditions. Additionally, we apply this bias voltage between the acquisition of two different I_{SC} data points when the spectra are changed for different z. This reduces the change in $I_{SC,top}$ of the perovskite solar cell. Since V_{MPP} is usually relatively close to V_{OC} and far away from 0 V and the ion distribution is similar under V_{MPP} and V_{OC},[29] we do not bias the solar cell with V_{MPP} but with V_{OC}. This simplifies the measurement procedure since no MPP tracking is necessary.

2.2.3. Circumventing Measurement Artifacts due to Low Parallel Resistance

Even though $V_{terminal} = 0$ V for measurements of $I_{SC}(z)$, the voltages of the subcells V_{top} and V_{bot} will not be zero if both subcells are not current-matched. In fact, the limiting subcell operates at a reverse bias voltage $-V_{rev}$ while the other subcell operates under a forward bias voltage $+V_{rev}$ if $V_{terminal} = 0$ V.[21,29] This is displayed in **Figure 3**a. This effect can influence the measurement of I_{SC}. Due to the finite parallel resistance of the limiting subcell $R_{p,lim}$, the current of the limiting subcell $I_{sub,lim}(V)$ at its point of operation $V_{sub,lim} = -V_{rev}$ will be larger than at its subcell short-circuit condition: $I_{sub,lim}(V_{sub,lim} = -V_{rev}) > I_{sub,lim}(V_{sub,lim} = 0$ V$)$. In consequence, $I_{SC,tandem} > I_{SC,sub,lim}$ because $I_{SC,tandem} := I_{tandem}$ $(V_{tandem} = 0$ V$) = I_{sub,lim}(-V_{rev}) > I_{sub,lim}(V_{sub,lim} = 0$ V$) =: I_{SC,sub,lim}$. This is displayed in Figure 3b. However, to determine the current
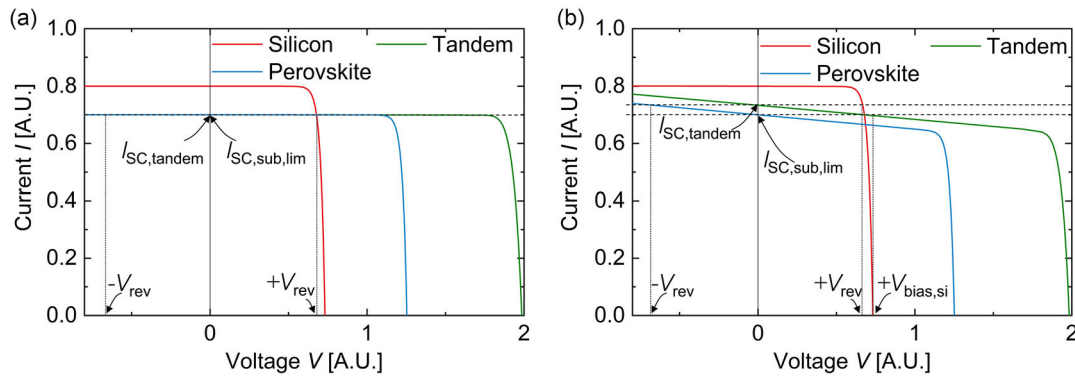
Figure 3. a) Schematic IV curves of a two-terminal dual-junction solar cell with high R_p which is not current-matched. The perovskite cell limits in this example. That means that at short-circuit of the tandem ($V_{terminal} = 0$), the perovskite subcell operates at $-V_{rev}$ and the silicon subcell operates at $+V_{rev}$. Since in this example R_p is high, $I_{SC,tandem} \approx I_{SC,sub,lim}$. b) Schematic IV curves of a two-terminal dual-junction solar cell with low R_p which is not current-matched. The perovskite cell limits in this example. Since $R_{p,sub,lim}$ of the limiting perovskite subcell is low, $I_{SC,tandem}$ is higher than $I_{SC,sub,lim}$. As indicated in the plot, $I_{SC,sub,lim}$ can be measured at the tandem IV curve at the correct bias voltage $V_{bias,sj} = +V_{rev}$. Since $+V_{rev}$ is not easy to determine, $V_{bias,si} = V_{oc,si} \approx +V_{rev}$ is used for the measurement of $I_{SC,sub,lim}$, introducing a negligible error.

matching point, $I_{SC,sub,lim}$ needs to be determined and not $I_{SC,tandem}$ (In fact, the subcell currents at MPP $I_{MPP,top}$ and $I_{MPP,bot}$ and not $I_{SC,top}$ and $I_{SC,bot}$ are of interest to find the point of maximum power for a dual-junction solar cell with low R_p. However, while it can make sense to measure a dual-junction solar cell with low R_p for future process optimization, it should always be the aim to optimize the production of the solar cells for well-performing solar cells with high R_p. In consequence, we do not consider the effect in this work that for low R_p the point of maximum power in the spectrum z_{MPP} shifts away from the current matching point z_{match}). To serve this requirement, an external bias voltage $V_{bias} = +V_{rev}$ needs to be applied to the dual-junction solar cell during the current measurement to extract $I_{SC,sub,lim}$, if $R_{p,lim}$ is too small. Only if $R_{p,lim}$ is sufficiently large, this effect can be neglected and $I_{SC,tandem} \approx I_{SC,sub,lim}$.

In this publication, this effect is considered for the perovskite silicon dual-junction solar cells, and a bias voltage is applied at the terminals during the measurements. For the measurement of I_{SC} when the perovskite subcell is the limiting subcell, a bias voltage $V_{bias,si} = +0.7\,V \approx V_{OC,si}$ is applied to compensate for the voltage of the silicon solar cell that operates close to its V_{OC} condition, as was suggested by Er-raji, Messmer et al.[28] This way, $I_{SC,pero}$ and not $I_{SC,tandem}$ is measured. For the measurement of I_{sc} when the silicon subcell is the limiting subcell, a bias voltage of $V_{bias,pero} = V_{OC,tandem} - 0.7\,V \approx V_{OC,pero}$ is applied to compensate for the voltage of the perovskite solar cell that operates close to its V_{OC} condition. This way, $I_{SC,si}$ and not $I_{SC,tandem}$ is measured. We use $V_{OC,tandem}$ and $V_{OC,si}$ to approximate $V_{OC,pero}$, as was also discussed in Er-raji, Messmer et al.[28] because those voltages are easier to access.

2.2.4. Postmeasurement Corrections

Usually, it is attempted to stabilize the spectrum of a solar simulator (independent of the applied light source) as good as possible and then measure the $I_{SC}(z)$ or IV curve of the solar cell under the targeted solar simulator spectrum. While this is the most precise approach, it costs time to wait until the light source is stable when moving on to the next spectrum. Not only the start of the solar simulator lamp, but also a change in light intensity between different spectra can lead to shifts in the light intensity due to, for example, temperature effects of the lamp. This holds true for LEDs as well as for the laser-based measurement system. However, the use of light sources such as lasers with narrow and nonoverlapping light emission spectra allows to precisely monitor the actual light intensity of each laser individually using two monitor diode units. This allows to correct the measured $I_{SC}(z)$ for the slight deviations in light intensity from the desired spectrum instead of waiting for the light source to become perfectly stable. Any deviation in the desired photocurrents of the two light sources leads to a change in the measured $I_{SC}(z)$ and can be described by two effects and their superposition: 1) a change of the overall light intensity of the combined spectrum of all light sources increasing or decreasing the current in both subcells simultaneously, expressed by a scaling factor A_{spec} for the spectrum and 2) a red- or blueshift in the spectrum increasing the current in one subcell while decreasing the current in the other subcell and vice versa. The latter effect causes a change of z. In contrast to the desired current densities j_{top}^{sim} and j_{bot}^{sim}, the real current densities $j_{top,real}^{sim}$ and $j_{bot,real}^{sim}$ can then be described introducing z_{real} and A_{spec} as displayed in (7) and (8).

$$j_{top,real}^{sim} = A_{spec}(1 + z_{real})j_{top}^{sim,AM1.5g} \tag{7}$$

$$j_{bot,real}^{sim} = A_{spec}(1 - z_{real})j_{bot}^{sim,AM1.5g} \tag{8}$$

Introducing the coefficients $A_{k,z,real}$ to describe the real laser spectrum $E_{k,z,real}(\lambda) = A_{k,z,real}e_k(\lambda)$, we can adapt the equation system of (5) and (6) to (9) and (10), highlighting changes in bold:

$$\sum_{k=1}^{2} C_{\text{top}} A_{k,z,\text{real}} \int s_{\text{top}}(\lambda) e_k d\lambda \tag{9}$$

$$= A_{\text{spec}}(1 + z_{\text{real}}) C_{\text{top}} \int s_{\text{top}}(\lambda) E_{\text{AM1.5g}}(\lambda) d\lambda$$

$$\sum_{k=1}^{2} C_{\text{bot}} A_{k,z,\text{real}} \int s_{\text{bot}}(\lambda) e_k d\lambda \tag{10}$$

$$= A_{\text{spec}}(1 - z_{\text{real}}) C_{\text{bot}} \int s_{\text{bot}}(\lambda) E_{\text{AM1.5g}}(\lambda) d\lambda$$

Note that $A_{1,z,\text{real}}$ and $A_{2,z,\text{real}}$ are known from the laser monitor diodes. Hence, the linear equation system in (9) and (10) can be solved for z_{real} and A_{spec}.

As mentioned above, we aim to keep the sum of the ratio of the subcell currents R_{top} and R_{bot} constant for all measurements, that is, $R_{\text{top}} + R_{\text{bot}} = 2$. However, this is violated with the introduction of A_{spec} in (7) and (8) for $A_{\text{spec}} \neq 1$. As **Figure 4** displays, the 1D measurement space along the line $R_{\text{top}} + R_{\text{bot}} = 2$ consequently becomes a 2D measurement space spanned by the two axes R_{top} and R_{bot}. Along any line that intersects with the point $R_{\text{top}} = R_{\text{bot}} = 0$ in Figure 4, such as the dashed line, the ratio $R_{\text{top}}/R_{\text{bot}}$ remains constant. Only the intensity (height) of the spectrum is changed along such a line, but the spectrum is not red- or blueshifted. In contrast, the sum of the subcell current ratios $R_{\text{top}} + R_{\text{bot}}$ remains constant along any line parallel to the solid line in Figure 4. Moving along the solid line red- or blueshifts the spectrum. For the correction of any measurement datapoint, this implies the following: The measurement data point $I_{\text{SC,meas}}(z_{\text{real}})$ can be shifted along the dashed line where $R_{\text{top}}/R_{\text{bot}} = \text{const}$ using $I_{\text{SC}}(z) = I_{\text{SC,meas}}(z)/A_{\text{spec}}$ ensuring $R_{\text{top}} + R_{\text{bot}} = 2$ after the correction. For this, we assume that the current of the subcells changes linearly with the incoming
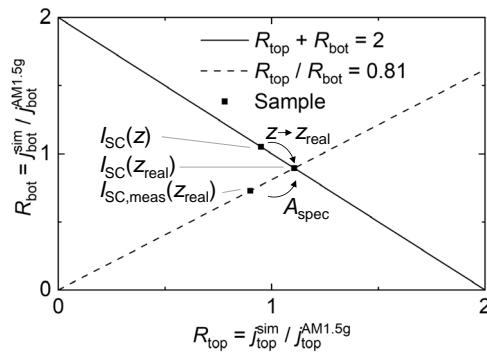

Figure 4. Visualization of the 2D space of spectral irradiance conditions. Adapted from Meusel et al.[10] R_{top} and R_{bot} describe the ratio of the current in the top and bottom cell under the simulated spectrum compared to the AM1.5g reference spectrum. Along any line that intersects with the point $R_{\text{top}} = R_{\text{bot}} = 0$, such as the dashed line does, the ratio $R_{\text{top}}/R_{\text{bot}}$ remains constant. Along such a line only the intensity/height of the spectrum is changed but it is not shifted to red or blue. The sum of the subcell current ratios $R_{\text{top}} + R_{\text{bot}}$ remains constant along the solid line, while the spectrum is red- or blueshifted. The correction procedure described above for each measured short-circuit current datapoint is visualized. While it was targeted to measure $I_{\text{SC}}(z)$, $I_{\text{SC,meas}}(z_{\text{real}})$ was measured due to variations in the light source. $I_{\text{SC,meas}}(z_{\text{real}})$ is corrected to $I_{\text{SC}}(z_{\text{real}})$ along the dashed line using the factor A_{spec}.
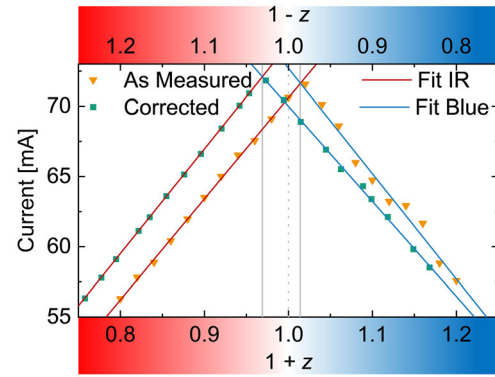

Figure 5. Exemplary measurement data showing the quick spectrometric measurement before the adjustment procedure is applied and after the measurement values are corrected. The correction of the measured current to fulfill the requirement $R_{\text{top}} + R_{\text{bot}} = 2$ (see Figure 4 for further explanation) leads to a vertical shift of the datapoints. The correction of z to z_{real} that the measured current is attributed to leads to a horizontal shift of the data points. Since the corrected data points follow the line of the fits more accurately than the raw data, most of the scattering in the measurement data can be traced back to variations in the light intensities. The two gray lines mark the current matching point of the as-measured and the corrected data. The gray dotted line marks the position of the AM1.5g spectrum. The measurement was conducted on a stable III–V dual-junction solar cell further described in the Supporting Information.

photon current in the relevant range. Attributing $I_{\text{SC}}(z)$ to z_{real} instead of the originally targeted z results in the final corrected data point $I_{\text{SC}}(z_{\text{real}})$. This procedure is also visualized in Figure 4.

Figure 5 shows the application of this correction procedure to a spectrometric measurement of a III–V dual-junction solar cell. The measurements were performed on purpose without light source stabilization. Hence, a large difference between the uncorrected data points and the datapoints corrected for variations in the illumination spectra is visible. Note that the corrected datapoints are much more aligned on the fit line than the uncorrected measurement datapoints. This indicates the success of the correction method and gives a hint that the fluctuation of the raw datapoints is due to the instability of the light source.

3. Results and Discussion

3.1. Method Validation

Perovskite silicon tandem solar cells are known to show transient effects, making them unsuitable for validating measurements. Hence, a quick spectrometric measurement was conducted on a stable III–V solar cell to validate the measurement method. The device is further described in the Supporting Information and in Dimroth et al.[32] The EQE of this solar cell is given in Figure S1, Supporting Information. The results of the quick spectrometric measurement are compared to a spectrometric measurement using an LED-based solar simulator conducted with the conventional method.[33] The results are shown in **Figure 6**. Both measurements took place with no bias voltage since the solar cell under test shows a high R_p with no significant influence on the current matching point. We find a deviation in
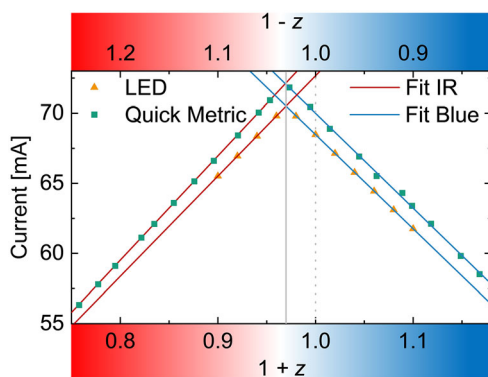
Figure 6. Validation of the measurement method. A conventional spectrometric measurement using an LED-based solar simulator and a quick spectrometric measurement are performed on a III–V dual-junction solar cell. The determined current matching point $1 + z_{match} = 0.97$ (solid gray line) is the same for both measurement methods within the measurement uncertainty discussed in the Supporting Information, while the current under current-matched conditions deviates by 2.3% (72.1 mA for the quick spectrometric measurement vs 70.5 mA for the conventional spectrometric measurement). The dotted gray vertical line marks the position of the AM1.5g spectrum.

Figure 7. Application of the method to two different perovskite silicon tandem solar cells. While sample 1 is almost current-matched under the AM1.5g spectrum ($1 + z_{match,sample1} = 0.98$), sample 2 is strongly perovskite limited ($1 + z_{match,sample2} = 1.11$). The gray dotted vertical line marks the position of the AM1.5g spectrum. The two gray solid lines mark the current matching point of sample 1 and sample 2.

the maximum current under current matching condition of 2.3% (72.1 mA for the quick spectrometric measurement versus 70.5 mA for the conventional spectrometric measurement). Accounting for the measurement uncertainties discussed in the Section S2, Supporting Information, and considering that the measurements were conducted on completely different measurement setups, this is a reasonable deviation. The same current matching point at $1 + z_{match} = 0.97$ is found for both measurement methods within the measurement uncertainties discussed in the Section S2, Supporting Information. This shows that the quick spectrometric measurement method is precise and well suited for quick scans of a large number of samples to detect, e.g., production failures—the purpose of the suggested method. No fundamental reasons prevent a higher precision of the new measurement method. Hence, measurement system adaptions to improve, e.g., the light spot homogeneity or the temperature control would certainly allow to further increase the precision of the quick spectrometric measurement setup. A conventional measurement should be conducted to investigate few samples very closely. Having complete IV curves at hand allows to detect, for example, if a defect or transient behavior of the perovskite solar cell causes an unexpected shape of the IV curve. Unexpected failures of the sample, which manifest in the shape of the IV curve, would not be noticed in the quick spectrometric measurement, where only $I_{SC}(z)$ is recorded.

3.2. Application to Perovskite Silicon Dual-Junction Solar Cells

The quick spectrometric method is applied to two different perovskite silicon dual-junction solar cells. For both solar cells, the perovskite layer is deposited on silicon heterojunction subcells using evaporation processes. The detailed structure of the solar cells is displayed in Figure S2, Supporting Information, with a detailed description of the processing steps
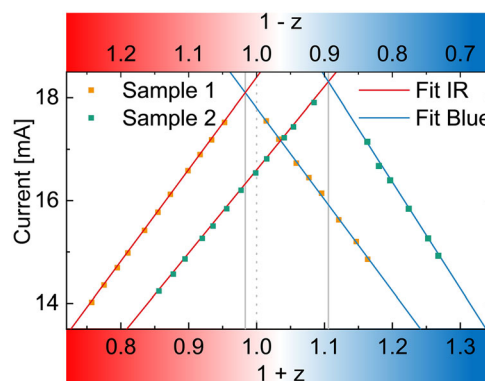
in the Section S1.2, Supporting Information. As **Figure 7** shows, sample 1 is slightly silicon limited under the AM1.5g spectrum and has a current matching point at $1 + z_{match,sample1} = 0.98$. On the contrary, sample 2 is strongly perovskite limited under the AM1.5g spectrum with a current matching point at $1 + z_{match,sample2} = 1.11$. Sample 2 was produced during a run-in process of the evaporation tool, where the optimal evaporation parameters had yet to be determined. The slight silicon limitation of sample 1 occurred due to variations in the production processes. These findings were confirmed by the determination of the bandgap, using a luminescence quantum yield measurement system. The perovskite top cell of sample 1 was found to have a bandgap of 1.65 eV while sample 2 has a bandgap of 1.7 eV. The shape of the EQE in Figure S3, Supporting Information, shows the same trend, explaining the low current of sample 2 in Figure S4, Supporting Information. A change in the thickness between the two samples changing the current matching point could be excluded since sample 1 and sample 2 have about the same thickness according to SEM measurements on similar substrates in Figure S5, Supporting Information.

These exemplary perovskite silicon dual-junction solar cells emphasize the importance of the quick spectrometric measurement method. The time-consuming conventional spectrometric measurement is usually only applied to a selection of samples. Since the variation in the current matching point in sample 1 was accidental, it might have been overlooked without the availability of the quick spectrometric measurement method. Also, the run-in process of the evaporation tool can be supported by the quick spectrometric measurement method since this method allows to test a significantly larger number of samples than the time-consuming conventional spectrometric measurement method. Due to a non-negligible R_p that was present in the IV characteristics of samples 1 and 2 in Figure S4, Supporting Information, a bias voltage of $V_{bias} = 0.7$ V and $V_{bias} = V_{OC,tandem} - 0.7$ V was applied for the perovskite and silicon limited measurements, respectively. In consequence, there is a gap between the datapoints of the perovskite and silicon limiting side close to the current matching point in Figure 7.

4. Conclusion and Outlook

In this work, we present a quick spectrometric characterization method to determine the current matching point of monolithic perovskite silicon dual-junction solar cells. Measuring I_{SC} instead of a full IV curve for each spectrum reduces the measurement duration compared to conventional spectrometric measurements significantly. Further reduction of the measurement duration is achieved by correcting for temporal deviations in the solar simulator spectrum rather than stabilizing the spectrum over a long time. Tracking temporal deviations in the solar simulator spectrum is simplified by using a solar simulator based on two lasers instead of multiple LEDs. The newly suggested method enables a high sample throughput and allows to determine the current limiting subcell or the current matching point within minutes instead of hours. Also, the short measurement duration of the quick spectrometric measurement method reduces the risk that the sample under test degrades during the measurement, rendering the measurement results invalid. The conventional spectrometric measurements can complement the quick spectrometric characterization method for a small number of stable samples. Recording the full IV curve, the conventional method allows for a more detailed analysis of selected dual-junction solar cells. From those, further information such as FF or hysteresis can be extracted. The quick spectrometric measurement method was validated by a measurement comparison to conventional spectrometric measurements using a stable III–V dual-junction solar cell. A deviation of 2.3% in the current at the current matching point was found for the quick spectrometric measurements compared to conventional spectrometric measurements on an LED-based solar simulator. This is a well acceptable deviation, taken that a prototype setup was used for the quick spectrometric measurements. Also, there are no fundamental reasons that prevent a higher precision of the new measurement method with an optimized setup.

Supporting Information

Supporting Information is available from the Wiley Online Library or from the author.

Author Contributions

Oliver Fischer and **Alexander J. Bett** developed the measurement method and designed the experiments. **Khusan Abrorov** characterized the measurement system and helped to quantify and decrease measurement uncertainties to a minimum. **Mohamed A. A. Mahmoud** processed the perovskite silicon dual-junction solar cells and performed the SEM measurements. **Florian Schindler**, **Stefan W. Glunz**, and **Martin C. Schubert** supervised the work. All authors contributed to the discussion of the results and reviewed the manuscript.

Data Availability Statement

The data that support the findings of this study are available from the corresponding author upon reasonable request.

Conflict of Interest

The authors declare no conflict of interest.

[1] Fraunhofer ISE, Photovoltaics Report, https://www.ise.fraunhofer.de/content/dam/ise/de/documents/publications/studies/Photovoltaics-Report.pdf (accessed: September 2024).

[2] M. A. Green, E. D. Dunlop, M. Yoshita, N. Kopidakis, K. Bothe, G. Siefer, D. Hinken, M. Rauer, J. Hohl-Ebinger, X. Hao, *Prog. Photovoltaics* **2024**, *32*, 425.

[3] T. Niewelt, B. Steinhauser, A. Richter, B. Veith-Wolf, A. Fell, B. Hammann, N. E. Grant, L. Black, J. Tan, A. Youssef, J. D. Murphy, J. Schmidt, M. C. Schubert, S. W. Glunz, *Sol. Energy Mater. Sol. Cells* **2022**, *235*, 111467.

[4] S. De Wolf, J. Holovsky, S.-J. Moon, P. Löper, B. Niesen, M. Ledinsky, F.-J. Haug, J.-H. Yum, C. Ballif, *J. Phys. Chem. Lett.* **2014**, *5*, 1035.

[5] P. Gao, M. Grätzel, M. K. Nazeeruddin, *Energy Environ. Sci.* **2014**, *7*, 2448.

[6] J.-P. Correa-Baena, A. Abate, M. Saliba, W. Tress, T. Jesper Jacobsson, M. Grätzel, A. Hagfeldt, *Energy Environ. Sci.* **2017**, *10*, 710.

[7] H. S. Jung, N. Park, *Small* **2015**, *11*, 10.

[8] E. Raza, Z. Ahmad, *Energy Rep.* **2022**, *8*, 5820.

[9] E. Aydin, T. G. Allen, M. De Bastiani, A. Razzaq, L. Xu, E. Ugur, J. Liu, S. De Wolf, *Science* **2024**, *383*, eadh3849.

[10] M. Meusel, R. Adelhelm, F. Dimroth, A. W. Bett, W. Warta, *Prog. Photovoltaics* **2002**, *10*, 243.

[11] A. J. Bett, D. Chojniak, M. Schachtner, S. K. Reichmuth, Ö. Kabaklı, P. S. C. Schulze, O. Fischer, F. Schindler, J. Hohl-Ebinger, G. Siefer, M. C. Schubert, *Sol. RRL* **2023**, *7*, 2200948.

[12] E. Aydin, T. G. Allen, M. De Bastiani, L. Xu, J. Ávila, M. Salvador, E. Van Kerschaver, S. De Wolf, *Nat. Energy* **2020**, *5*, 851.

[13] E. Köhnen, M. Jošt, A. B. Morales-Vilches, P. Tockhorn, A. Al-Ashouri, B. Macco, L. Kegelmann, L. Korte, B. Rech, R. Schlatmann, B. Stannowski, S. Albrecht, *Sustainable Energy Fuels* **2019**, *3*, 1995.

[14] E. Köhnen, P. Wagner, F. Lang, A. Cruz, B. Li, M. Roß, M. Jošt, A. B. Morales-Vilches, M. Topič, M. Stolterfoht, D. Neher, L. Korte, B. Rech, R. Schlatmann, B. Stannowski, S. Albrecht, *Sol. RRL* **2021**, *5*, 2100244.

[15] J. Xu, C. C. Boyd, Z. J. Yu, A. F. Palmstrom, D. J. Witter, B. W. Larson, R. M. France, J. Werner, S. P. Harvey, E. J. Wolf, W. Weigand, S. Manzoor, M. F. A. M. Van Hest, J. J. Berry, J. M. Luther, Z. C. Holman, M. D. Mcgehee, *Science* **2020**, *367*, 1097.

[16] L. Mazzarella, Y. Lin, S. Kirner, A. B. Morales-Vilches, L. Korte, S. Albrecht, E. Crossland, B. Stannowski, C. Case, H. J. Snaith, R. Schlatmann, *Adv. Energy Mater.* **2019**, *9*, 1803241.

[17] C. U. Kim, J. C. Yu, E. D. Jung, I. Y. Choi, W. Park, H. Lee, I. Kim, D.-K. Lee, K. K. Hong, M. H. Song, K. J. Choi, *Nano Energy* **2019**, *60*, 213.

[18] B. Chen, Z. Yu, K. Liu, X. Zheng, Y. Liu, J. Shi, D. Spronk, P. N. Rudd, Z. Holman, J. Huang, *Joule* **2019**, *3*, 177.

[19] A. Al-Ashouri, E. Köhnen, B. Li, A. Magomedov, H. Hempel, P. Caprioglio, J. A. Márquez, A. B. Morales Vilches, E. Kasparavicius, J. A. Smith, N. Phung, D. Menzel, M. Grischek, L. Kegelmann, D. Skroblin, C. Gollwitzer, T. Malinauskas, M. Jošt, G. Matič, B. Rech, R. Schlatmann, M. Topič, L. Korte, A. Abate, B. Stannowski, D. Neher, M. Stolterfoht, T. Unold, V. Getautis, S. Albrecht, *Science* **2020**, *370*, 1300.

[20] M. De Bastiani, A. J. Mirabelli, Y. Hou, F. Gota, E. Aydin, T. G. Allen, J. Troughton, A. S. Subbiah, F. H. Isikgor, J. Liu, L. Xu, B. Chen, E. Van Kerschaver, D. Baran, B. Fraboni, M. F. Salvador, U. W. Paetzold, E. H. Sargent, S. De Wolf, *Nat. Energy* **2021**, *6*, 167.

[21] M. Meusel, C. Baur, G. Létay, A. W. Bett, W. Warta, E. Fernandez, *Prog. Photovoltaics* **2003**, *11*, 499.

[22] J. Metzdorf, *Appl. Opt.* **1987**, *26*, 1701.

[23] M. Saliba, L. Etgar, *ACS Energy Lett.* **2020**, *5*, 2886.

[24] M. Mundus, B. Venkataramanachar, R. Gehlhaar, M. Kohlstädt, B. Niesen, W. Qiu, J. P. Herterich, F. Sahli, M. Bräuninger, J. Werner, J. Hohl-Ebinger, G. Uytterhoeven, U. Würfel, C. Ballif, M. C. Schubert, W. Warta, S. W. Glunz, *Sol. Energy Mater. Sol. Cells* **2017**, *172*, 66.

[25] R. Adelhelm, K. Bücher, *Sol. Energy Mater. Sol. Cells* **1998**, *50*, 185.

[26] M. Heydarian, C. Messmer, A. J. Bett, M. Heydarian, D. Chojniak, Ö. Kabaklı, L. Tutsch, M. Bivour, G. Siefer, M. C. Schubert, J. C. Goldschmidt, M. Hermle, S. W. Glunz, P. S. C. Schulze, *Sol. RRL* **2023**, *7*, 2200930.

[27] Ö. Kabaklı, J. Kox, L. Tutsch, M. Heydarian, A. J. Bett, S. Lange, O. Fischer, C. Hagendorf, M. Bivour, M. Hermle, P. S. C. Schulze, J. C. Goldschmidt, *Sol. Energy Mater. Sol. Cells* **2023**, *254*, 112246.

[28] O. Er-Raji, C. Messmer, A. J. Bett, O. Fischer, S. K. Reichmuth, F. Schindler, M. Bivour, O. Schultz-Wittmann, J. Borchert, M. Hermle, J. Schön, F. D. Heinz, M. C. Schubert, P. S. C. Schulze, S. W. Glunz, *Sol. RRL* **2023**, *7*, 2300659.

[29] C. Messmer, D. Chojniak, A. J. Bett, S. K. Reichmuth, J. Hohl-Ebinger, M. Bivour, M. Hermle, J. Schön, M. C. Schubert, S. W. Glunz, *Prog. Photovoltaics* **2024**, https://doi.org/10.1002/pip.3782.

[30] J. Thiesbrummel, V. M. Le Corre, F. Peña-Camargo, L. Perdigón-Toro, F. Lang, F. Yang, M. Grischek, E. Gutierrez-Partida, J. Warby, M. D. Farrar, S. Mahesh, P. Caprioglio, S. Albrecht, D. Neher, H. J. Snaith, M. Stolterfoht, *Adv. Energy Mater.* **2021**, *11*, 2101447.

[31] Y. Liu, C. Xie, W. Tan, X. Liu, Y. Yuan, Q. Xie, Y. Li, Y. Gao, *Org. Electron.* **2019**, *71*, 123.

[32] F. Dimroth, R. Beckert, M. Meusel, U. Schubert, A. W. Bett, *Prog. Photovoltaics* **2001**, *9*, 165.

[33] D. Chojniak, M. Schachtner, S. K. Reichmuth, A. J. Bett, M. Rauer, J. Hohl-Ebinger, A. Schmid, G. Siefer, S. W. Glunz, *Prog. Photovoltaics* **2024**, *32*, 372.